Taylor & Francis
Taylor & Francis Group

ORIGINAL RESEARCH

∂ OPEN ACCESS | Check for updates

Dipeptidyl peptidase 4 inhibition sensitizes radiotherapy by promoting T cell infiltration

Yu Tian[a,b]*, Lingyi Kong[a,b]*, Yan Li[a,b], Zhiyun Liao[a,b], Xing Cai[a,b], Suke Deng[a,b], Xiao Yang[a,b], Bin Zhang[a,b], Yijun Wang[a,b], Zhanjie Zhang[a,b], Bian Wu[a,b], Lu Wen[a,b], Fang Huang[a,b], Yan Hu[a,b], Chao Wan[a,b], Yifei Liao[c], Yajie Sun[a,b], and Kunyu Yang[a,b,d]

[a]Cancer Center, Union Hospital, Tongji Medical College, Huazhong University of Science and Technology, Wuhan, China; [b]Hubei Key Laboratory of Precision Radiation Oncology, Wuhan, China; [c]Division of Infectious Diseases, Department of Medicine, Brigham and Women's Hospital, Harvard Medical School, Boston, MA, USA; [d]Institute of Radiation Oncology, Union Hospital, Tongji Medical College, Huazhong University of Science and Technology, Wuhan, China

ABSTRACT

Radiotherapy could regulate systemic antitumor immunity, while the immune state in the tumor micro-environment (TME) also affects the efficacy of radiotherapy. We have found that higher CD8$^+$ T cell infiltration is associated with longer overall survival of lung adenocarcinoma and melanoma patients receiving radiotherapy. 8-Gray radiation increased the transcriptional levels of chemokines in tumor cells *in vitro*. However, it was not sufficient to induce significant lymphocyte infiltration *in vivo*. Dipeptidyl peptidase 4 (DPP4) has been reported to inactivate chemokines via post-translational truncation. Single-cell sequencing revealed that dendritic cells (DCs) had a higher DPP4 expression among other cells in the TME and upregulated DPP4 expression after radiation. Combining a DPP4 inhibitor with radiotherapy could promote chemokines expression and T cell infiltration in the TME, enhancing the antitumor effect of radiotherapy. Moreover, this therapy further enhanced the therapeutic efficacy of anti-PD-1. In this study, we demonstrated the underlying mechanism of why radiotherapy failed to induce sufficient T cell infiltration and proposed an effective strategy to promote T cell infiltration and sensitize radiotherapy. These findings demonstrate the translational value of DPP4 inhibition as a complementary approach to enhance the efficacy of radiotherapy and the combination of radiotherapy with immunotherapy.

Introduction

Radiotherapy is a well-established treatment modality for malignant tumors, with 50%–70% of patients requiring it for either cure or local control during their treatment process.[1] Radiotherapy has been shown to contribute to the anti-tumor immune response through various mechanisms, including inducing an "*in situ* vaccine effect",[2,3] altering the immuno-genicity of tumor cells,[4] and reprogramming the tumor microenvironment (TME) from an immunosuppressive "cold tumor" phenotype to an immunostimulatory "hot tumor" phenotype.[5,6] By inducing the expression and secre-tion of pro-inflammatory cytokines and chemokines, radia-tion can recruit pro-inflammatory immune cells.[7–9] Immune cell infiltration, especially T cell infiltration, plays a critical role in immune checkpoint blockade (ICB) therapy, indicat-ing that immune cell chemotaxis after radiation may be a key factor contributing to the synergistic effects of radiotherapy and immunotherapy.[10,11] *In vitro* studies have demonstrated that irradiation (IR) promotes the expression of chemokines in tumor cells, indicating its potential to attract T cells to migrate into the tumor site.[12] However, several studies, including the clinical trial (NCT03223155), reported that no

significant increase in T cell infiltration was observed after radiotherapy *in vivo*.[13,14] This suggests the presence of unknown mechanisms that negatively regulate chemokines in the TME, limiting the radiation-induced immune response.

The degradation of chemokines and cytokines, such as being cleaved by proteases and enzymes, is the primary mechanism responsible for their inactivation *in vivo*.[15] Dipeptidyl Peptidase 4 (DPP4), also known as T cell surface marker CD26, is a widely expressed transmembrane glyco-protein that recognizes proteins with proline or alanine at the penultimate position and cleaves the amino-terminal dipeptides to modulate protein structure and function.[16] Numerous chemokines and cytokines serve as potential substrates for DPP4.[17,18] *In vitro* studies have shown that DPP4 cleaves CXCL10 to produce a product that acts as an antagonist to its receptor CXCR3, thereby attenuating its chemotactic effect.[19,20] Promising results from studies focusing on DPP4 suppression in melanoma, liver, breast, colon, and pancreatic tumors hint at future clinical applications.[19,21–26] However, there exists a notable gap in research concerning the effectiveness and underlying

mechanisms of DPP4 inhibitors in the context of radiotherapy.

In this study, we aim to identify the distribution of DPP4 expression after radiotherapy, elucidate the role of DPP4 in radioresistance, and validate the therapeutic efficacy of combining DPP4 inhibition with radiotherapy. Our findings showed that dendritic cells (DCs) constituted the predominant cell subpopulation with high DPP4 expression in the TME. Additionally, we observed that DPP4 expression in DCs hindered the chemotaxis of immune cells following radiotherapy *in vitro*. When radiotherapy was combined with DPP4 inhibitor treatment, a significant increase in T cell infiltration was observed, leading to the inhibition of tumor growth and an improved therapeutic response to anti-PD-1 antibody treatment.

Materials and methods

Chemicals and Antibodies

Vildagliptin (LAF-237, DPP4 inhibitor) and anti-CD8 antibody were purchased from Selleck. Anti-PD-1 antibody was purchased from BioXcell.

Cell culture

Murine B16F10 melanoma cell line, murine Lewis lung carcinoma cell line (LLC) and murine 4T1 breast cancer cell line were purchased from the American Tissue Culture Collection. Luciferase stably transfected B16F10-LUC cell line was established and maintained in our laboratory.

Radiation

Cells were exposed to a single dose of 8-Gray (Gy) radiation, following which the culture medium was replaced with fresh medium. Subsequently, mice, bearing tumors on their posterior limbs, were anesthetized with a 1% pentobarbital sodium solution and irradiated with a single dose of 8 Gy each time. During cell radiation, culture plates were positioned on a 1 cm thick plastic platform, with a radiation field measuring 40×40 cm. Similarly, for mouse tumor radiation, the animals were placed on a 1 cm thick plastic platform, and the posterior limbs bearing tumors were exposed to a radiation field measuring 40×2 cm, carefully avoiding exposure to normal tissues. All dose delivery was performed by the beam quality of 6 MV and dose rate of 6 Gy/min (600 MU/min, Trilogy System Linear Accelerator, Varian Medical Systems).

Real-time quantitative polymerase chain reaction (RT-qPCR)

Total RNA was extracted from cells using the Total RNA Kit I R6834 (Omega) and was subjected to complementary DNA synthesis using HiScript III RT SuperMix (Vazyme), following the manufacturer's instructions. The RT-qPCR reaction was performed using AceQ Universal SYBR qPCR Master Mix (Vazyme) on a StepOnePlus Real-Time PCR System (Thermo Fisher Scientific). All primers used in this study were synthesized by Sangon Biotech Co. Ltd. and were listed in Table S1.

Generation of bone marrow-derived dendritic cells (BMDCs) and bone marrow-derived macrophages (BMDMs)

For the generation of BMDCs and BMDMs, bone marrow cells collected from femurs of C57BL/6 mice were cultured in the complete RPMI 1640 medium, in the presence of granulocyte-macrophage colony-stimulating factor (GM-CSF, 20 ng/ml; Biolegend) or macrophage colony-stimulating factor (M-CSF, 20 ng/ml; PeproTech), respectively. Red blood cells (RBCs) were depleted using RBC lysis buffer (Biosharp). The culture medium was replaced with fresh medium every 2 days. BMDCs and BMDMs were harvested on the seventh day for further experiments.

Single-cell RNA sequencing

After euthanizing the LLC subcutaneous tumor mice 72-h post-8 Gy irradiation, both the irradiated and control tumor-bearing mice were submerged in 75% alcohol. Following a 10-minute immersion, they were transferred to a sterile laminar flow hood. With the use of sterilized scissors and forceps, the subcutaneous tumor tissues were meticulously separated and gathered (ensuring the sampled tissues were free from necrosis or blood clots). These tissues were then cut into small pieces, approximately 100 mg in size, washed twice with sterile PBS buffer, and promptly submerged in pre-chilled tissue preservation solution (GEXSCOPE TM Tissue Preservation Solution, Singleron). Then, samples were sent to Singleron Biotechnologies Inc. for single-cell library construction, scRNA-sequencing, and data analysis.

For tissue dissociation and preparation, the samples were digested with 3 mL sCellLiveTM Tissue Dissociation Solution (Singleron) by Singleron PythoN™ Tissue Dissociation System at 37°C for 15 min. The cell suspension was collected and filtered through a 40-micron sterile strainer. Afterward, the GEXSCOPE® red blood cell lysis buffer (RCLB, Singleron) was added, and the mixture [Cell: RCLB = 1:2 (volume ratio)] was incubated at room temperature for 5–8 min to remove red blood cells. The mixture was then centrifuged at 300 g at 4°C for 5 mins to remove supernatant and suspended softly with PBS. Finally, the samples were stained with Trypan Blue and the cell viability was evaluated microscopically.

For RNA isolation and cDNA library construction, Single-cell suspensions (2×10^5 cells/mL) with PBS (HyClone) were loaded onto microwell chip using the Singleron Matrix® Single Cell Processing System. Barcoding Beads are subsequently collected from the microwell chip, followed by reverse transcription of the mRNA captured by the Barcoding Beads and to obtain cDNA, and PCR amplification. The amplified cDNA is then fragmented and ligated with sequencing adapters. The scRNA-seq libraries were constructed according to the protocol of the GEXSCOPE® Single Cell RNA Library Kits (Singleron). Individual libraries were diluted to 4 nM, pooled, and sequenced on Illumina nova-seq 6000 with 150 bp paired-end reads.

Raw reads from scRNA-seq were processed to generate gene expression matrixes using CeleScope (https://github.com/sin gleron-RD/CeleScope) v1.9.0 pipeline. Briefly, raw reads were first processed with CeleScope to remove low-quality reads with Cutadapt v1.17 to trim poly-A tail and adapter sequences. Cell barcodes and unique molecular identifiers (UMIs) were extracted. After that, STAR v2.6.1a was used to map reads to the reference genome GRCm38 (ensemble version 92 annotation). UMIs counts and gene counts of each cell were acquired with feature Counts v2.0.1 software, and used to generate expression matrix files for subsequent analysis.

Immune cells profiling by Flow Cytometry (FC)

Mice tumor tissues were cut into small pieces and digested with 0.32 mg/mL collagenase Ⅴ (Biosharp) and 0.5 mg/mL hyaluronidase (Biosharp) for 1 h, then grinding the digested tissues. Cells were then washed with PBS and resuspended in PBS for further experiments. For FC, single-cell suspensions were stained with Zombie to exclude dead cells. To analyze BMDCs and BMDMs, cell suspensions were stained with CD45, CD11b, CD11c, CD86, CD80, and F4/80 antibodies at 4°C for 30 min.

To analyze T cells, cell suspensions were stained with CD3, CD4, and CD8a. For T cell intracellular cytokine staining, cell suspensions were first stimulated with Phorbol 12-myristate 13-acetate (PMA) (100 ng/mL; Abcam), Monensin sodium salt (1 μg/mL; Abcam), and Ionomycin calcium salt (100 ng/mL; MCE) for 4–6 h before fixation and permeabilization, then were stained with IFN-γ, GrzB and FOXP3 antibodies at 4°C for 30 min.

All antibodies for FC were purchased from BioLegend and were listed in Table S2.

Cell chemotaxis assay

Tumor cells with or without a single dose of 8 Gy radiation were seeded into twelve-well Transwell plates. Single-cell suspensions made from spleens were seeded into 3 μm Transwell upper chambers and were cocultured with cells in twelve-well plates for 24 h. The serum-free medium from unirradiated and irradiated B16F10 cells and applied with or without vildagliptin to BMDCs for 6 h. The culture medium was then collected and centrifuged to remove cells and cell fragments, which was next supplemented with serum and filtered to get the conditioned medium. The control or conditioned medium in the lower chamber. Single-cell suspensions made from spleens were seeded into upper chambers and were cocultured with cells in twelve-well plates for 24 h before FC.

Tumor tissue proinflammatory chemokines detection

Mice tumor tissue was harvested and processed according to the manufacturer's instructions. Chemokines in mice tumor tissues were quantified by LEGENDplex Mouse Proinflammatory Chemokine Panel (BioLegend) using FC.

Animal experiments and evaluation of therapeutic effects

Mice used for experiments were 6-week and sex-matched mice. C57BL/6, Balb/c and Balb/c-nude mice were purchased from SJA Laboratory Animal Co. (Hunan, China). All animals were maintained in the specific pathogen-free barrier facility in the Animal Center of Huazhong University of Science and Technology (HUST; Wuhan, China). All animal studies were performed in compliance with protocols that had been approved by the Hubei Provincial Animal Care and Use Committee, in accordance with the experimental guidelines of the Animal Experimentation Ethics Committee of the HUST (Wuhan, China). The IACUC Number was 3209. To establish the subcutaneous transplanted B16F10-LUC and LLC tumor model, 5×10^5 cells were injected subcutaneously into the right flank of female C57BL/6. For 4T1 tumor model, 5×10^5 cells were injected subcutaneously into the right flank of Balb/c and Balb/c-nude. When the tumor volume reached about 50 mm³, mice were divided randomly into four groups. Mice were treated with vildagliptin (20 mg/kg) or PBS via gastric gavage every 2 days with or without irradiation with a single dose of 8 Gy. Subcutaneous tumor sizes were measured by vernier calipers and recorded based on the length (L) and the width (W) of tumors. Tumor volume (V) was calculated with the formula $V = (L \times W^2/2)$.

Bioluminescence imaging

Mice were intraperitoneally injected with firefly luciferin (150 mg/kg; Sigma-Aldrich) after being anesthetized with 1% pentobarbital sodium. After 15 min, the luminescent images were acquired with a 3-min exposure time, and X-ray photographs were taken with a 30-s exposure time by a Bruker In Vivo MS FX PRO Imager.

CD8⁺ T cell depletion assay

On the day before treatment, 200 μg of mouse anti-CD8 antibodies per mouse were intraperitoneally injected. The second dose was given 3 days later with 150 μg of antibodies per mouse.

Statistical analysis

Statistical analysis was performed with GraphPad Prism 9.0 software. For comparisons of two groups, statistical significance was analyzed using two-tailed unpaired Student's t-test. For comparisons of three or more groups, one-way analysis of variance (ANOVA) with Tukey's multiple-comparison test was performed. Results were presented as mean ± standard error mean (SEM). *: $p < .05$; **: $p < .01$; ***: $p < .001$; and ns, not significant.

Results

IR fails to recruit T cells in vivo

Preexisting CD8⁺ T cells are vital for the efficacy of immunotherapy, while it remains controversial whether radiation promotes CD8⁺ T cell infiltration. Initially, we explored the

relationship between CD8^{+} T cells in the TME and the response to radiotherapy using The Cancer Genome Atlas (TCGA) database. We selected the patients with lung adenocarcinoma (LUAD) and cutaneous melanoma (SKCM) who received radiotherapy and had available transcriptome data. The infiltration of CD8^{+} T cells in the TME was determined by the CIBERSORT algorithm. As shown in Figure 1a–b, a higher percentage of CD8^{+} T cells in the TME was associated with prolonged survival in LUAD and SKCM patients. Furthermore, as our primary approach involved palliative radiotherapy for stage IV patients rather than radical radiotherapy for *in situ* tumors, we conducted an analysis that excluded stage IV patients. This analysis revealed that patients with a higher proportion of CD8^{+} T cells in the TME experienced extended survival, and this difference remained statistically significant in SKCM patients (Fig. S1a-S1b).

It has been reported that irradiation could increase chemokines secretion.[12] We demonstrated that the transcription of CXCL9 and CXCL10 was upregulated in both LLC and melanoma B16F10 cells after 8-Gy irradiation (Figure 1c–d and Fig. S1c-S1d). To further examine whether irradiated tumor cells could recruit immune cells, we performed a Transwell experiment. Spleen cells were collected from the lower chamber after co-culture with unirradiated or irradiated (8 Gy) LLC and B16F10 cells (Figure 1e). FC was used to identify the types of immune cells recruited by tumor cells. Irradiated LLC and B16F10 cells recruited more CD45^{+} immune cells, and specifically significantly higher levels of CD4^{+} T and CD8^{+} T cells were recruited after 8 Gy irradiation (Figure 1f–g). Additionally, we sorted CD8^{+} T cells from spleen and performed the Transwell experiment. As shown in Fig. S1e-S1f, irradiated (8 Gy) LLC and B16F10 cells recruited more CD8^{+} T cells *in vitro*. However, the recruited CD8^{+} T cells did not exhibit significant differences in the expression of CD69, LAG3 and PD-1.

The above data showed that irradiated tumor cells induced chemotaxis of T cells *in vitro*. Subsequently, we investigated the T cell recruitment effect of irradiation (IR) *in vivo*. We established a subcutaneous transplanted tumor model of B16F10 in C57BL/6 mice. The mice were randomly divided into two groups after the tumor volume reached approximately 50 mm^3. One group was treated with a single dose of 8 Gy radiation. One week later, the mice were sacrificed, and tumors were harvested. Immunofluorescence (IF) showed that irradiation did not increase the fraction of CD8^{+} T cells *in vivo* (Figure 1h–i). We also used FC to analyze the changes in T cells in the TME after irradiation. The gating strategy is shown in Fig. S1e. Unlike the *in vitro* results, irradiation did not significantly increase either the fraction of Th1 (CD4^{+}IFN-γ^{+}) and CTL (CD8^{+}IFN-γ^{+}, CD8^{+}GrzB^{+}) or the percentage of CD4^{+} and CD8^{+} T cells (Figure 1j–k and Fig. S1h-S1k). Interestingly, we observed that irradiation significantly increased the fraction of regulatory T cells (Treg, CD4^{+}FoxP3^{+}) (Fig. S1k). Although irradiated tumor cells increased the expression of chemokines and recruitment of T cells *in vitro*, IR failed to recruit T cells in this mouse model. Therefore, it is vital to study the mechanism behind this phenomenon and propose an effective method to promote T cell infiltration *in vivo*.
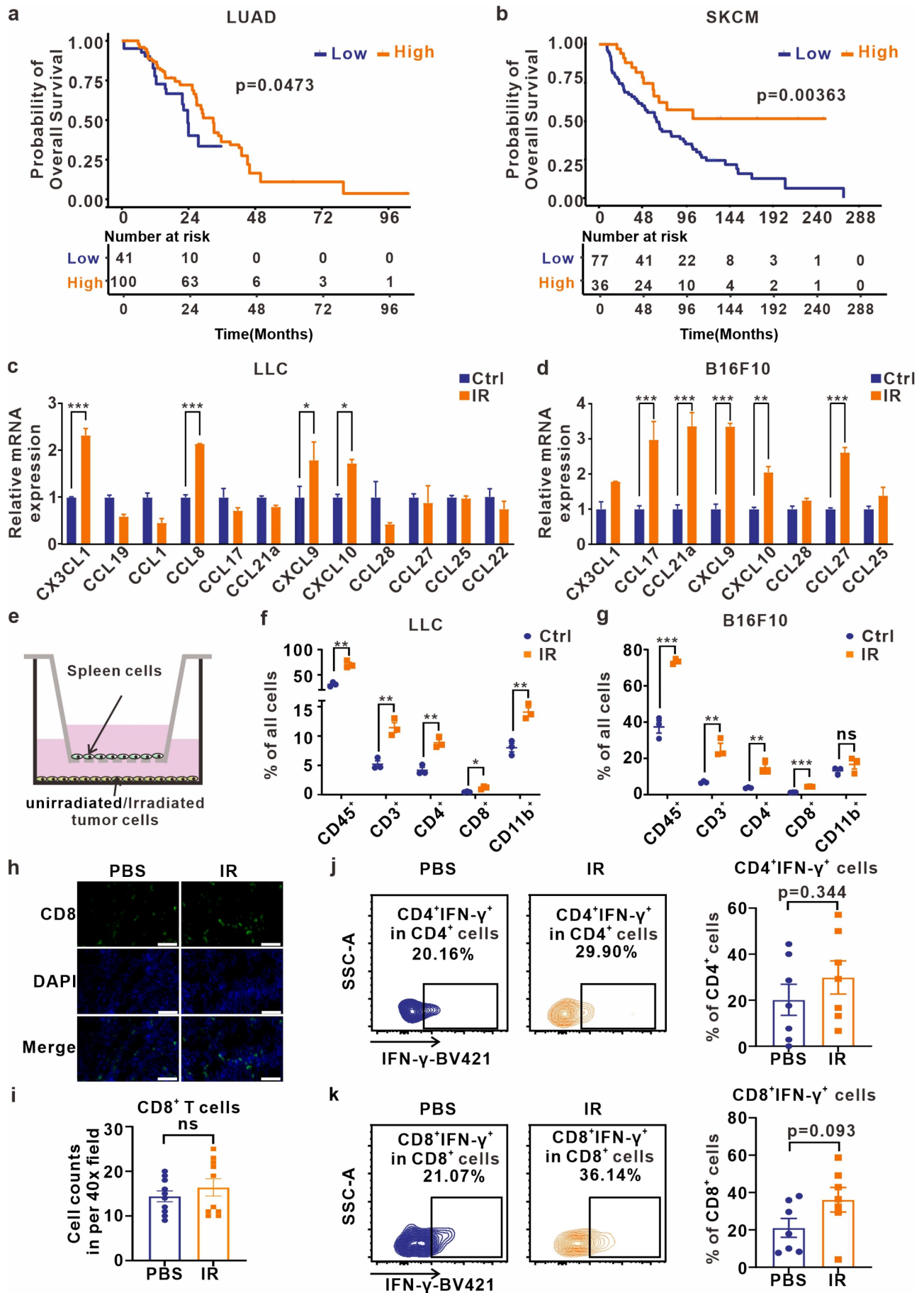
IR increases DPP4 expression in DCs

Chemokines play a pivotal role in influencing lymphocyte infiltration into the TME. Our results showed that radiotherapy promotes the expression of chemokines and the recruitment of immune cells *in vitro*. However, this effect was not observed in a mouse model, prompting us to investigate whether chemokines were inactivated *in vivo*. Twelve chemokines, including CXCL9, CXCL10, CCL5, and CCL11, have been identified as substrates of DPP4, a serine exopeptidase that inhibits the function of chemokines via cleavage. To explore the role of DPP4 in T cell infiltration, we initially measured the expression of DPP4 in the TME. We analyzed two datasets of SKCM in the Tumor Immune Single-cell Hub2 (TISCH2). As shown in Figure 2a–b and Fig. S2a-S2b, DCs exhibited the highest DPP4 expression in both databases. To validate the data, we used FC to analyze the DPP4 levels in various cell types within B16F10-LUC tumors. Our analysis included macrophages (CD45^{+}CD11b^{+}F4/80^{+} cells), DCs (CD45^{+}CD11c^{+} cells), CD3^{+} T cells, CD8^{+} T cells, and tumor cells (CD45^{−} cells), with DCs showing the highest DPP4 expression in mouse tumors (Figure 2c–d). Additionally, we confirmed these findings through RT-qPCR, which indicated that BMDCs had the highest mRNA levels compared to LLC, B16F10, and BMDMs (Figure 2e–f). Immunoblot results further supported the RT-qPCR findings (Fig. S2d).

To profile the changes in DPP4 expression after IR, we performed single-cell RNA sequencing (scRNA-seq) for LLC control tumors and irradiated (8 Gy) tumors. The scRNA-seq results revealed that DPP4 was primarily expressed in DCs and was upregulated in DCs following IR (Figure 2g–h). FC results also indicated an upregulation of DPP4 levels in DCs after 8 Gy radiation (Figure 2i). To further study how IR upregulates DPP4 in DCs, we tested the direct effect of IR on DPP4 expression in DCs and found that IR did not directly affect the DPP4 levels in DCs (Figure 2j). Since IR could induce immunogenic cell death of tumor cells and activate DCs *in vivo*, we explored whether the upregulation of DPP4 was related to DC activation. We collected conditioned medium (CM) from tumor cells or irradiated (8 Gy) tumor cells, then cultured BMDCs with either CM or lipopolysaccharide (LPS). We found that LPS treatment and CM from both unirradiated and irradiated tumor cells significantly increase the DPP4 expression on BMDCs. Notably, CM from irradiated tumor cells exhibited the highest potential for inducing DPP4 expression (Figure 2k and S2e-S2f). Furthermore, we discovered a positive correlation between DPP4 mRNA levels in DCs and the expression of DCs activation markers CD80 and CD86 in the scRNA-seq database (Figure 2l–m and S2g-S2h).

Vildagliptin enhances tumor response to IR

We then investigated whether the inhibition of DPP4 enzyme activity in BMDCs, using the effective and specific DPP4 inhibitor, vildagliptin, could enhance the chemotaxis of T cells. We collected serum-free medium from unirradiated and irradiated (8 Gy) B16F10 cells and applied it to BMDCs with or without vildagliptin for 6 h. The culture medium was subsequently collected, centrifuged to remove

a LUAD

b SKCM

c LLC

d B16F10

e

f LLC

g B16F10

h

i CD8⁺ T cells

j CD4⁺IFN-γ⁺ cells

k CD8⁺IFN-γ⁺ cells

cells and cell fragments, supplemented with serum, and filtered to obtain the conditioned medium. This conditioned medium was added to the lower chamber, while spleen cells were placed in the upper chamber (Figure 3a). Compared to unirradiated B16F10, irradiated B16F10 cells promoted T cell infiltration and myeloid cell chemotaxis to the lower chamber (Figure 3b–f). Additionally, the medium from BMDCs inhibited T cell recruitment, which could be rescued by the addition of vildagliptin (Figure 3b–f).

To further explore the effect of vildagliptin in sensitizing IR, we performed the preclinical experiment using B16F10-LUC cells, LLC, 4T1, and MC38 (Figure 3g). In the B16F10 subcutaneous model, combining vildagliptin with a single dose of 8 Gy radiation significantly inhibited the tumor growth and reduced tumor weight (Figure 3h–i). Similarly, in the LLC, 4T1, and MC38 subcutaneous models, vildagliptin enhanced the tumor response to 8 Gy radiation (Figure 3j–k and Fig. S3a-S3d). Taken together, our results showed that vildagliptin inhibited tumor growth in combination with 8 Gy radiation. Furthermore, we assessed the biocompatibility of vildagliptin in combination with 8 Gy radiation in healthy mice. Three days after the last administration, the blood and tissue were collected for biochemical analysis and hematoxylin-eosin staining. There were no significant differences in the number of red blood cells (RBC) and white blood cells (WBC) among mice from different treatment groups (Figure 3l). To evaluate liver and kidney function, we measured alanine transaminase (ALT), aspartate aminotransferase (AST), blood urea nitrogen (BUN), and creatinine (CR). No significant differences were observed among the four groups (Fig. S3e-S3h). Additionally, histopathological examination of lung, heart, kidney, and liver revealed normal histological morphology in the combined treatment group (Fig. S3i). Therefore, these data indicated that vildagliptin is safe in combination with IR.

Vildagliptin promotes T cell infiltration in combination with IR

To understand the mechanisms of vildagliptin, we first examined the effect of vildagliptin on tumor cells and BMDCs in vitro. As shown in Fig. S4a-S4b, vildagliptin did not directly induce tumor cell death, whether with or without 8 Gy irradiation. In BMDCs, vildagliptin did not increase the expression of CD80 and CD86, nor affect the LPS-induced upregulation of CD80 and CD86 (Fig. S4c-S4d). Since DPP4 is known to inactivate chemokines, we then explored whether vildagliptin could affect the level of chemokines in the TME in vivo. We harvested tumors as indicated in Fig. S5a-S5b and measured the chemokine concentration in the TME by LEGENDplex. Compared to 8 Gy radiation treatment alone, the combination group significantly increased the expression of CXCL9, CXCL10, and CCL2, which involved in the recruitment of

T cells. Furthermore, the combination group also promoted cytokines that contribute to the recruitment of other immune cells, such as CXCL13, CCL11, CXCL1, and CCL3/CCL4 for B cells, eosinophil, neutrophil, and monocytes, respectively (Figure 4a and S5c-S5j).

To clarify the changes in the immune microenvironment after different treatments in vivo, we measured immune cells in the TME by FC. We observed a significant increase of CD3$^+$, CD4$^+$, and CD8$^+$ T cells in the combination group (Figures 4b–e). Additionally, Th1 and CTL populations were significantly increased in the combination group (Figures 4f–h), while no difference in Treg cells was observed among the four groups (Figure 4i). IF also showed a significant increase in CD8+ T cells in the combination group (Fig S5k-S5l). We also used 8 Gy × 3 radiation to test whether vildagliptin could sensitize tumors to radiotherapy in vivo. Vildagliptin enhanced the tumor response to IR in the B16F10 model (Fig. S6a-S6b). Higher dose radiation increased the CD8$^+$ T cell infiltration compared to the PBS group. While the combination group had the highest CD4$^+$ and CD8$^+$ T cells (Fig. S6c-S6f). In addition, the Th1 and CTL were significantly increased in the combination group (Fig. S6g-S6h). Collectively, these results demonstrate that vildagliptin promotes T cell infiltration in combination with IR.

To evaluate the role of adaptive immunity in the antitumor activity of combination treatment, we performed the animal experiment in Balb/c nude mice using 4T1 cells (Fig. S7a). In nude mice, the vildagliptin was not capable of enhancing the antitumor effect of IR, suggesting that the radiosensitization effect of vildagliptin depends on adaptive immunity (Fig. S7b). To further investigate the role of CD8$^+$ T cells in the antitumor activity of combination treatment. We depleted CD8$^+$ T cells using anti-CD8 antibody (Fig. S7c). The depletion efficiency of CD8$^+$ T cells in blood and spleen exceeded 99% (Fig. S7d-S7e). The inhibitory effect of the combination was reversed in mice that underwent CD8$^+$ T cell depletion (Figures 4j–l), suggesting that the antitumor effect of combination treatment predominantly relies on CD8$^+$ T cells.

Vildagliptin sensitizes the combination of radiotherapy and immunotherapy.

As demonstrated earlier, the combination of vildagliptin and IR promoted T cell infiltration and activated antitumor immunity. We then examined if the combination treatment could further increase the efficacy of immunotherapy (Figure 5a). As shown in Figures 5b–d and Fig. S8a-8b, the triple combination of a single dose of 8-Gy radiation, vildagliptin, and anti-PD-1 significantly inhibited the tumor growth compared to control, anti-PD-1 alone and the combination of IR and vildagliptin. Furthermore, immunohistochemistry showed that the triple combination group had the highest level of CD8$^+$ T cells

---

Figure 1. IR promotes expression of chemokines in tumor cells but fails to recruit T cells in vivo. (a) Kaplan – Meier curves for overall survival of LUAD patients according to the level of CD8$^+$ T cell infiltration. (b) Kaplan – Meier curves for overall survival of SKCM patients according to the level of CD8$^+$ T cell infiltration. (c-d) RT-qPCR analysis of the relative mRNA levels of chemokines in LLC and B16F10 cells treated by IR. (e) Schematic of the Transwell experiment. (f-g) The percentage of recruited immune cells by irradiated LLC and B16F10 in the lower chamber was determined by FC. (h) Representative images of CD8$^+$ T cells in B16F10 subcutaneous tumors. Scale bar = 50 μm. (i) The summary of CD8$^+$ T cells in each field. (j-k) FC analysis of indicated T cell subset in the tumors with PBS and IR treatment (n = 7).
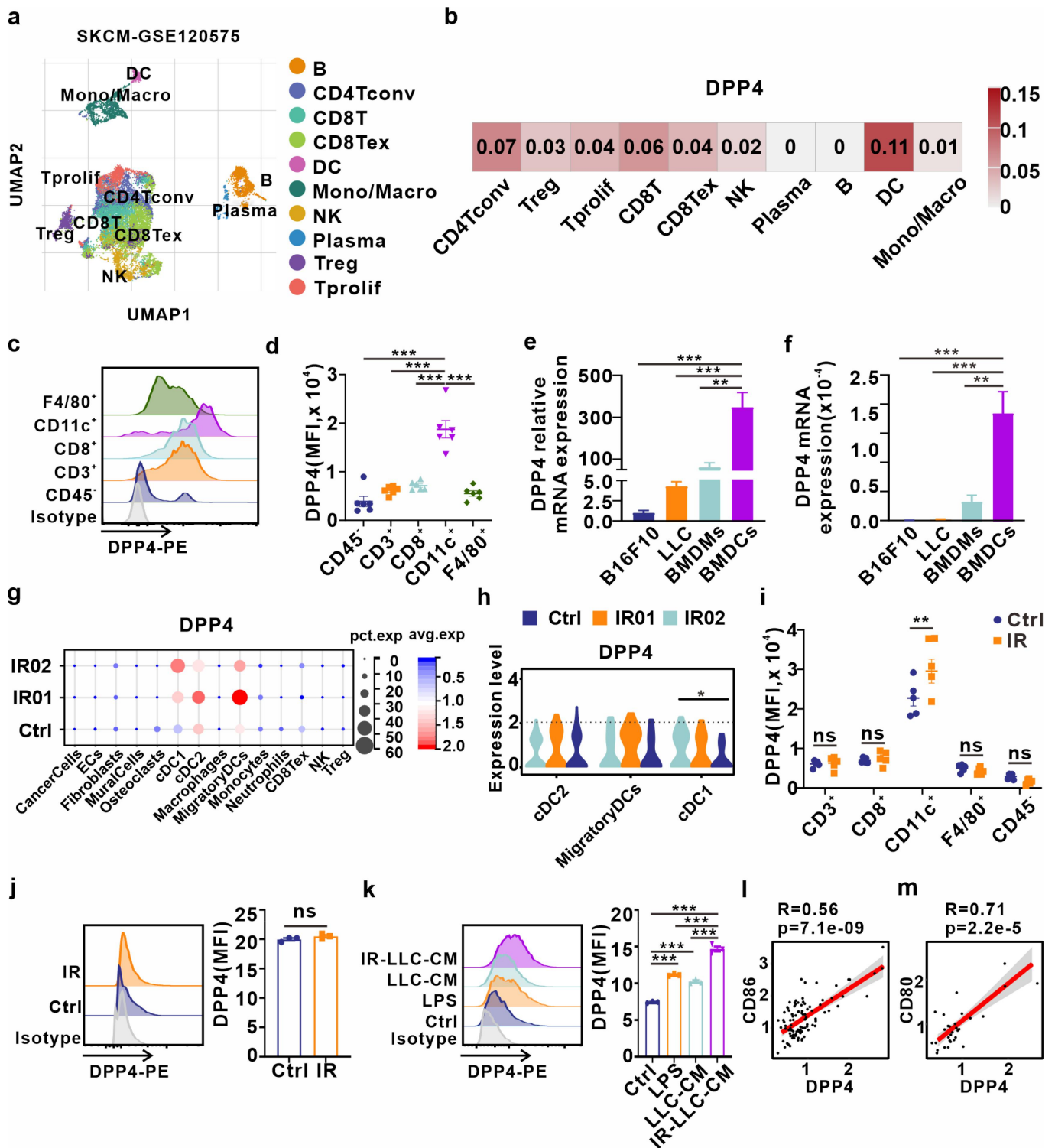
Figure 2. IR upregulates DPP4 expression in DCs. (a) Uniform Manifold Approximation and Projection (UMAP) plots of SKCM with 10 TME clusters. (b) Heat map of DPP4 levels in each cell cluster. (c-d) FC analysis of DPP4 expression in various cell types in tumors of B16F10-LUC mice. MFI, mean fluorescence intensity. (e-f) RT-qPCR analysis of the DPP4 expression in B16F10, LLC, BMDMs and BMDCs. (g) Bubble plot showing the expression of DPP4 in each cell type within the tumors of LLC mice with or without IR. (h) Violin plot of DPP4 expression in cDC2, migratory-DCs and cDC1 within the tumor of LLC mice with or without IR. (i) Flow cytometric analysis of DPP4 expression in various cell types in tumor of B16F10-LUC mice with or without IR. (j) FC analysis of DPP4 expression in the BMDCs with or without IR. Antibody isotype was included as a control. (k) FC analysis of DPP4 expression in the BMDCs with LPS, LLC- CM and IR-LLC-CM. (l-m) The scatter plot and correlation between the DPP4 expression and CD86 expression (l) or CD80 expression (m) in the DCs of pan-cancer scRNA-seq database.

(Figure 5e), and IF revealed that the triple combination therapy led to the highest proportion of apoptotic cells (Fig. S7c-7d).

Given the promising results of the triple combination therapy in the preclinical model, we explored whether vildagliptin could further enhance the combination of 8 Gy × 3 radiation and anti-PD-1 to activate the antitumor immunity and inhibit the formation and growth of distant tumors. After the treatment, we subcutaneously injected
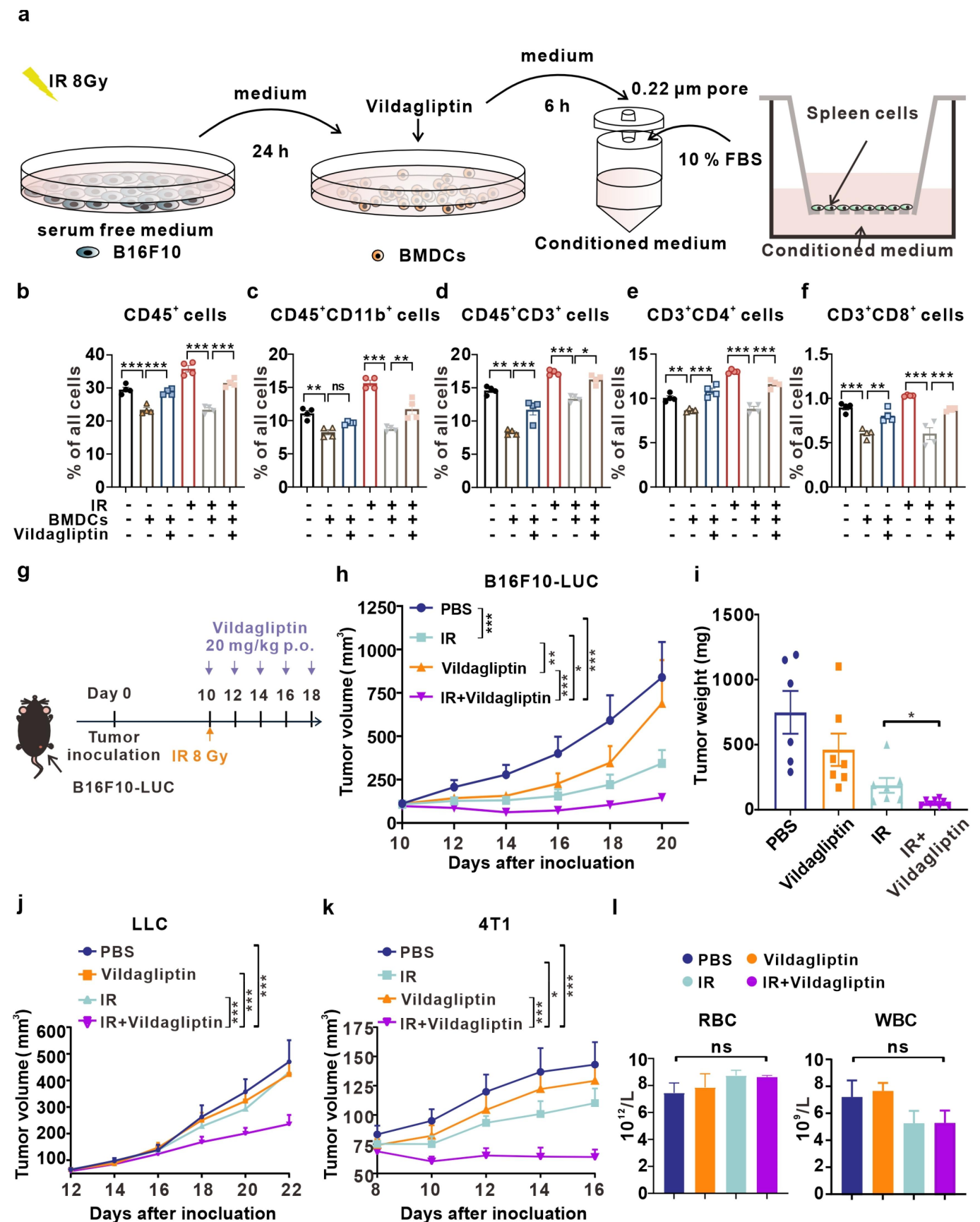
a

b CD45+ cells **c** CD45+CD11b+ cells **d** CD45+CD3+ cells **e** CD3+CD4+ cells **f** CD3+CD8+ cells

g **h** B16F10-LUC **i**

j LLC **k** 4T1 **l**

Figure 3. Vildagliptin sensitizes radiotherapy. (a) Schematic of the Transwell experiment. (b-f) The percentage of recruited immune cells by conditioned medium in the lower chamber was determined by FC. (b) CD45+ cells, (c)myeloid cells (CD45+CD11b+), (d) T cells (CD45+CD3+), (e) CD4+ T cells (CD45+CD3+CD4+), (f) CD8+ T cells (CD45+CD3+CD8+) among the cells in the lower chamber. (g) Schematic of the treatment plan. (h) Tumor growth curves of B16F10-LUC cell subcutaneous transplant model in corresponding treatment groups (n = 6-8). (i) Tumor weight on day 20 after inoculation in (g). (j) Tumor growth curves of LLC cell subcutaneous transplant model in corresponding treatment groups (n = 8). (k) Tumor growth curves of 4T1 cell subcutaneous transplant model in corresponding treatment groups (n = 8). (l) Hemanalysis was performed on blood drawn from mice on day 3 after treatment. Red blood cells (RBC) and White blood cells (WBC) are presented as the means ± SEM (n = 5).
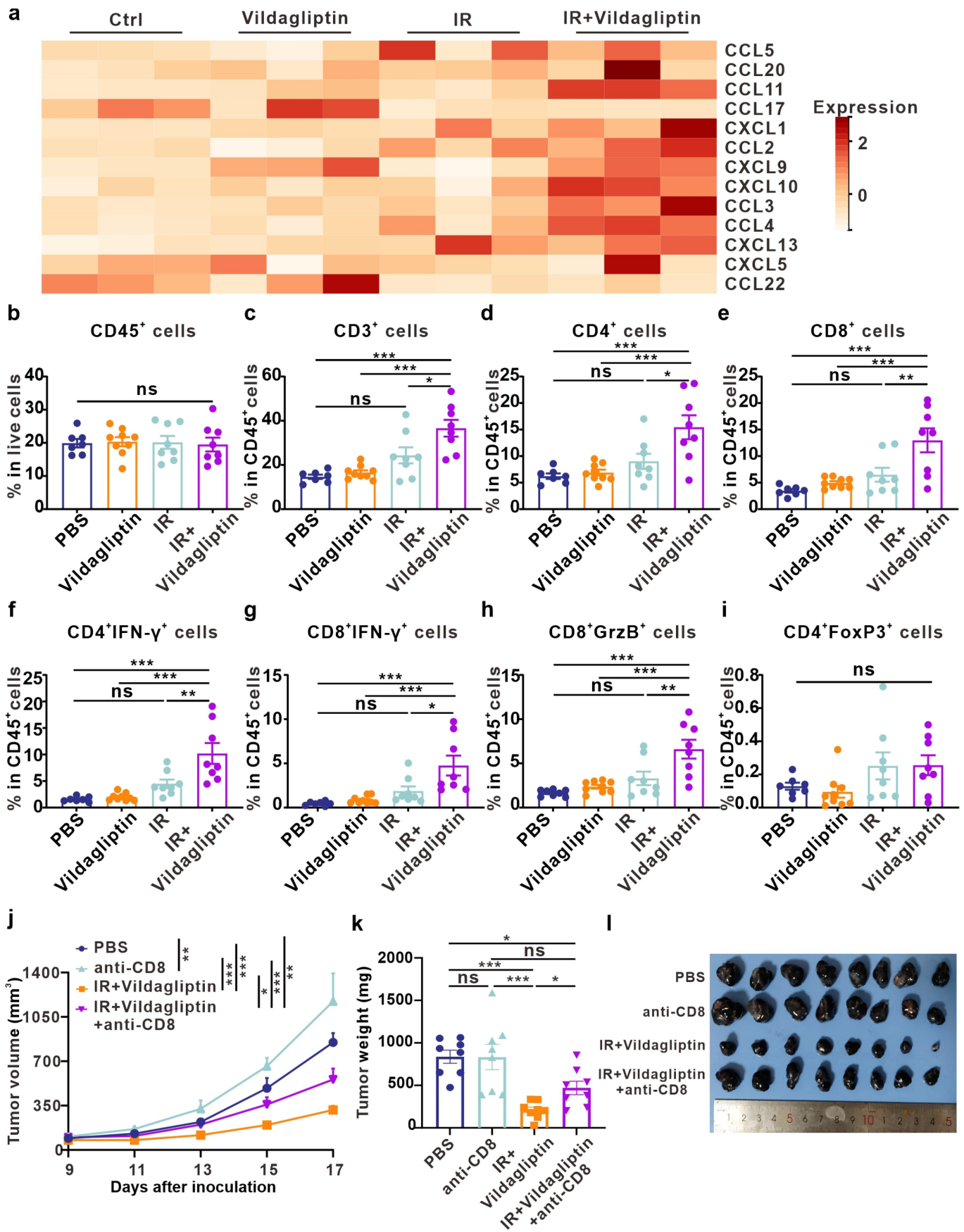
Figure 4. Combination of vildagliptin and IR promotes T cell infiltration. (a) Heat map of chemokines levels in the tumor after treatment as in (Fig. S5a). (b-i) FC analysis of each immune cell subset in the tumor after treatment as in (Fig. S5a). (b) Proportions of leukocytes (CD45$^+$) cells among live cells. (c) CD3$^+$ T cells, (d) CD4$^+$ T cells, (e) CD8$^+$ T cells, (f)Th1 (CD4$^+$ IFN-γ$^+$), (g) CTL (CD8$^+$IFN-γ$^+$), (h) CTL (CD8$^+$GrzB$^+$), (i) Tregs (CD4$^+$Foxp3$^+$) among CD45$^+$ cells. (j) Tumor growth curves of B16F10-LUC cell subcutaneous transplant model in corresponding treatment groups (*n* = 8). (k) Tumor weight on day 17 after inoculation in (j). (l) Photo of dissected tumors from each group in (j).
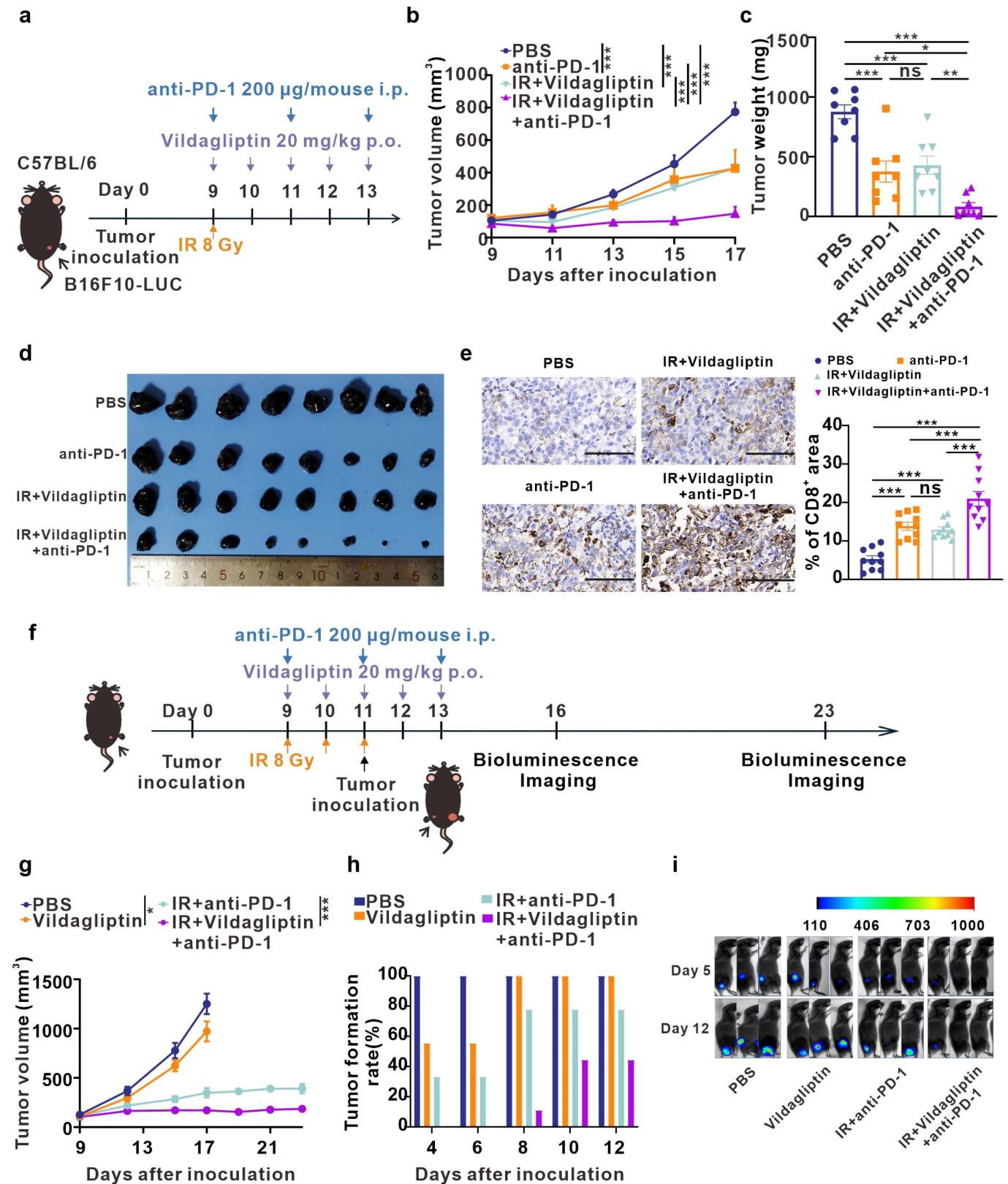
Figure 5. Vildagliptin sensitizes the combination of radiotherapy and immunotherapy. (a) Schematic of the treatment plan. (b) Tumor growth curves of B16F10-LUC cell subcutaneous transplant model in corresponding treatment groups ($n = 8$). (c) Tumor weight on day 17 after treatment in (a). (d) Photo of dissected tumors from each group in (a). (e) Representative images of CD8 immunohistochemical staining with blue representing nuclei and brown representing positive staining. Scale bar = 100 μm (left). The positive area of CD8$^+$ cells in each field (right). (f) Schematic of the treatment plan. (g) Tumor growth curves of the primary site of B16F10-LUC cell subcutaneous transplant model in corresponding treatment groups ($n = 6$-9). (h) The tumor formation rate of the secondary site of B16F10-LUC cell subcutaneous transplant model ($n = 6$-9). (i) Bioluminescence images of the secondary site in corresponding treatment groups.

B16F10-LUC on the other side and monitored its formation and growth (Figure 5f). For the primary tumor, we observed that the triple combination therapy exhibited the strongest tumor growth inhibition activity (Figure 5g). Regarding the secondary tumor, the triple combination therapy significantly prolonged the time to tumor formation (Figure 5h). When the tumor volume reached $50\,mm^3$, it was labeled as tumor formation. In the PBS group, all secondary tumors formed on day 4 after inoculation, whereas in the triple combination therapy group, only one tumor had formed on day 8 after inoculation (Figure 5h). Representative bioluminescence images of the secondary tumor growth are shown in Figure 5i. Taken together, these findings indicate that vildagliptin is a promising approach to sensitize radiotherapy and enhance the combination of radiotherapy and immunotherapy by activating system antitumor immunity.

Discussion

Radiotherapy exhibits both tumoricidal and immunomodulatory effects, making it a promising approach for synergistic antitumor therapy in combination with immunotherapy. However, radiotherapy cannot induce sufficient T cell infiltration, hindering its success in this combination treatment.[10,11,13,27] In our study, we found that radiation increased the expression of chemokines in tumor cells *in vitro* (Figure 1c–d). However, DPP4 expressed in BMDCs inactivated chemokines, causing insufficient T cell infiltration into tumor localization *in vivo* (Figure 3). To address this limitation, we investigated the mechanism by which inhibition of DPP4 sensitizes radiotherapy. Our results showed that the combination of radiotherapy and DPP4 inhibitor vildagliptin overcame this obstacle, as the combination therapy exhibited superior tumor-suppressive effects that the levels of chemokines and lymphocyte infiltration were significantly increased in the TME, and the tumor growth was efficiently limited (Figures 3–4). In addition, we utilized single-cell databases and scRNA-seq to profile the expression of DPP4 in the TME and found that DCs expressed high levels of DPP4, which could be further increased when co-cultured with irradiated tumor cells (Figure 2). These results provided insights into the possible regulatory system of DPP4. Thus, our study provides a theoretical basis for future combination therapy of DPP4 inhibitors and radiotherapy that could advance cancer treatment.

Moreover, our study revealed that the combination therapy of IR and the DPP4 inhibitor further enhanced the therapeutic efficacy of ICB. The response rate of ICB alone in clinical treatment is limited to 10%-30%, and most patients with malignancies hardly benefit from immunotherapy alone.[28,29] Therefore, combining ICB with other systemic or local therapies is currently under active investigation. It has been well demonstrated that the level of infiltrated lymphocytes in the TME is a crucial predictor of the response rate to ICB, and higher lymphocyte infiltration is associated with a higher response rate.[28] In our study, we first demonstrated that the combination of radiotherapy and vildagliptin significantly increased T cell infiltration in the TME. Therefore, we further combined this therapy with anti-PD-1 antibody for the treatment of B16F10-LUC melanoma mice. The results showed that the triple combination therapy effectively inhibited melanoma growth and distant tumor formation in mice (Figure 5). These findings suggest that the triple combination regimen of radiotherapy, vildagliptin, and ICB enhances the antitumor immunity and potentially has significant clinical translational value.

Previous studies by Matthew L Albert et al demonstrated that DPP4 inhibited the infiltration levels of T cells and eosinophils in the TME by truncating CXCL10 and CCL11 *in vivo*. The application of DPP4 inhibitors or DPP4 knockout mice promoted T cells and eosinophils infiltration, which in turn enhances the anti-tumor immune response.[21] These findings partially support our results. Since the DPP4 inhibitor class has been approved by the FDA, which means it is safe in the clinic. Our study provides a theoretical basis for combining DPP4 inhibitors with radiotherapy, advancing clinical trials of this drug in cancer treatment.

Although our study provides a promising novel combination therapy for cancer treatment, there are some questions that remain to be studied. The chemokine substrate of DPP4 in the TME remains to be identified and the molecular mechanism is unknown. Future studies will characterize the role of other immune cells in the combination therapy. Also, the benefit of DPP4 inhibitors in cancer treatment mostly stays in the status of preclinical study, let alone in the combination of radiotherapy and immunotherapy. Prospective and randomized clinical trials are needed for the clinical anticancer treatment of DPP4 inhibitors.

In summary, our study proposes a novel approach to improve the efficacy of radiotherapy in cancer treatment by inhibiting DPP4 enzyme activity, thus preventing chemokine inactivation and promoting T cell infiltration into the TME. The combination treatment modality effectively enhances the radiation-induced antitumor immunity and further improves the therapeutic effect of immunotherapy.

Disclosure statement

No potential conflict of interest was reported by the author(s).

Funding

Data availability statement

The authors confirm that the data supporting the findings of this study are available within the article and its supplementary materials.

References

1. Citrin DE, Longo DL. Recent developments in radiotherapy. N Engl J Med. 2017;377(11):1065–1075. doi:10.1056/NEJMra1608986.
2. Alexandrov LB, Nik-Zainal S, Wedge DC, Aparicio SAJR, Behjati S, Biankin AV, Bignell GR, Bolli N, Borg A, Børresen-Dale A-L, et al. Signatures of mutational processes in human cancer. Nature. 2013;500(7463):415–421. doi:10.1038/nature12477.
3. Rudqvist NP, Pilones KA, Lhuillier C, Wennerberg E, Sidhom J-W, Emerson RO, Robins HS, Schneck J, Formenti SC, Demaria S, et al. Radiotherapy and CTLA-4 blockade shape the TCR repertoire of tumor-Infiltrating T cells. Cancer Immunol Res. 2018;6(2):139–150. doi:10.1158/2326-6066.CIR-17-0134.
4. Reits EA, Hodge JW, Herberts CA, Groothuis TA, Chakraborty M.l.K., Wansley E, Camphausen K, Luiten, RM, de Ru, AH, Neijssen J, et al. Radiation modulates the peptide repertoire, enhances MHC class I expression, and induces successful antitumor immunotherapy. J Exp Med. 2006;203(5):1259–1271. doi:10.1084/jem.20052494.
5. Colton M, Cheadle EJ, Honeychurch J, Illidge TM. Reprogramming the tumour microenvironment by radiotherapy: implications for radiotherapy and immunotherapy combinations. Radiat Oncol. 2020;15(1):254. doi:10.1186/s13014-020-01678-1.
6. Sevenich L. Turning "cold" into "hot" tumors-opportunities and challenges for radio-immunotherapy against primary and metastatic brain cancers. Front Oncol. 2019;9:163. doi:10.3389/fonc.2019.00163.
7. Wan C, Sun Y, Tian Y, Lu L, Dai X, Meng J, Huang J, He Q, Wu B, Zhang Z, et al. Irradiated tumor cell–derived microparticles mediate tumor eradication via cell killing and immune reprogramming. Sci Adv. 2020;6(13):eaay9789. doi:10.1126/sciadv.aay9789.
8. Cytlak UM, Dyer DP, Honeychurch J, Williams KJ, Travis MA, Illidge TM. Immunomodulation by radiotherapy in tumour control and normal tissue toxicity. Nat Rev Immunol. 2022;22(2):124–138. doi:10.1038/s41577-021-00568-1.
9. Zhai D, Huang J, Hu Y, Wan C, Sun Y, Meng J, Zi H, Lu L, He Q, Hu Y, et al. Ionizing radiation-induced tumor cell-derived microparticles prevent lung metastasis by remodeling the pulmonary immune microenvironment. Int J Radiat Oncol Biol Phys. 2022;114(3):502–515. doi:10.1016/j.ijrobp.2022.06.092.
10. Dovedi SJ, Cheadle EJ, Popple AL, Poon E, Morrow M, Stewart R, Yusko EC, Sanders CM, Vignali M, Emerson RO, et al. Fractionated radiation therapy stimulates antitumor immunity mediated by both resident and infiltrating polyclonal T-cell populations when combined with PD-1 blockade. Clin Cancer Res. 2017;23(18):5514–5526. doi:10.1158/1078-0432.CCR-16-1673.
11. Arina A, Beckett M, Fernandez C, Zheng W, Pitroda S, Chmura SJ, Luke JJ, Forde M, Hou Y, Burnette B, et al. Tumor-reprogrammed resident T cells resist radiation to control tumors. Nat Commun. 2019;10(1):3959. doi:10.1038/s41467-019-11906-2.
12. Wang L, Jiang J, Chen Y, Jia Q, Chu Q. The roles of CC chemokines in response to radiation. Radiat Oncol. 2022;17(1):63. doi:10.1186/s13014-022-02038-x.
13. Chen HY, Xu L, Li LF, Liu XX, Gao JX, Bai YR. Inhibiting the CD8(+) T cell infiltration in the tumor microenvironment after radiotherapy is an important mechanism of radioresistance. Sci Rep. 2018;8(1):11934. doi:10.1038/s41598-018-30417-6.
14. Spurr LF, Martinez CA, Kang W, Chen M, Zha Y, Hseu R, Gutiontov SI, Turchan WT, Lynch CM, Pointer KB, et al. Highly aneuploid non-small cell lung cancer shows enhanced responsiveness to concurrent radiation and immune checkpoint blockade. Nat Cancer. 2022;3(12):1498–1512. doi:10.1038/s43018-022-00467-x.
15. Nagarsheth N, Wicha MS, Zou W. Chemokines in the cancer microenvironment and their relevance in cancer immunotherapy. Nat Rev Immunol. 2017;17(9):559–572. doi:10.1038/nri.2017.49.
16. Shao S, Xu Q, Yu X, Pan R, Chen Y. Dipeptidyl peptidase 4 inhibitors and their potential immune modulatory functions. Pharmacology & Therapeutics. 2020;209:107503. doi:10.1016/j.pharmthera.2020.107503.
17. Metzemaekers M, Van Damme J, Mortier A, Proost P. Regulation of chemokine activity - a focus on the role of Dipeptidyl peptidase IV/CD26. Front Immunol. 2016;7:483. doi:10.3389/fimmu.2016.00483.
18. Han CK, Lee WF, Hsu CJ, Huang Y-L, Lin C-Y, Tsai C-H, Huang C-C, Fong Y-C, Wu M-H, Liu J-F, et al. DPP4 reduces proinflammatory cytokine production in human rheumatoid arthritis synovial fibroblasts. J Cell Physiol. 2021;236(12):8060–8069. doi:10.1002/jcp.30494.
19. Barreira da Silva R, Laird ME, Yatim N, Fiette L, Ingersoll MA, Albert ML. Dipeptidylpeptidase 4 inhibition enhances lymphocyte trafficking, improving both naturally occurring tumor immunity and immunotherapy. Nat Immunol. 2015;16(8):850–858. doi:10.1038/ni.3201.
20. Decalf J, Tarbell KV, Casrouge A, Price JD, Linder G, Mottez E, Sultanik P, Mallet V, Pol S, Duffy D, et al. Inhibition of DPP4 activity in humans establishes its in vivo role in CXCL10 post-translational modification: prospective placebo-controlled clinical studies. EMBO Mol Med. 2016;8(6):679–683. doi:10.15252/emmm.201506145.
21. Hollande C, Boussier J, Ziai J, Nozawa T, Bondet V, Phung W, Lu B, Duffy D, Paradis V, Mallet V, et al. Inhibition of the dipeptidyl peptidase DPP4 (CD26) reveals IL-33-dependent eosinophil-mediated control of tumor growth. Nat Immunol. 2019;20(3):257–264. doi:10.1038/s41590-019-0321-5.
22. Nishina S, Yamauchi A, Kawaguchi T, Kaku K, Goto M, Sasaki K, Hara Y, Tomiyama Y, Kuribayashi F, Torimura T, et al. Dipeptidyl peptidase 4 inhibitors reduce hepatocellular carcinoma by activating lymphocyte chemotaxis in mice. Cell Mol Gastroenterol Hepatol. 2019;7(1):115–134. doi:10.1016/j.jcmgh.2018.08.008.
23. Fitzgerald AA, Wang S, Agarwal V, Marcisak EF, Zuo A, Jablonski SA, Loth M, Fertig EJ, MacDougall J, Zhukovsky E, et al. DPP inhibition alters the CXCR3 axis and enhances NK and CD8+ T cell infiltration to improve anti-PD1 efficacy in murine models of pancreatic ductal adenocarcinoma. J Immunother Cancer. 2021;9(11):e002837. doi:10.1136/jitc-2021-002837.
24. Qin CJ, Zhao LH, Zhou X, Zhang H-L, Wen W, Tang L, Zeng M, Wang M-D, Fu G-B, Huang S, et al. Inhibition of dipeptidyl peptidase IV prevents high fat diet-induced liver cancer angiogenesis by downregulating chemokine ligand 2. Cancer Lett. 2018;420:26–37. doi:10.1016/j.canlet.2018.01.064.
25. Huang XY, Zhang PF, Wei CY, Peng R, Lu J-C, Gao C, Cai J-B, Yang X, Fan J, Ke A-W, et al. Circular RNA circMET drives immunosuppression and anti-PD1 therapy resistance in hepatocellular carcinoma via the miR-30-5p/snail/DPP4 axis. Mol Cancer. 2020;19(1):92. doi:10.1186/s12943-020-01213-6.
26. Zhan ZT, Liu L, Cheng MZ, Gao Y, Zhou WJ, Xu B. The effects of 6 common antidiabetic drugs on anti-PD1 immune checkpoint inhibitor in tumor treatment. J Immunol Res. 2022;2022:1–24. doi:10.1155/2022/2651790.
27. Meng J, Li Y, Wan C, Sun Y, Dai X, Huang J, Hu Y, Gao Y, Wu B, Zhang Z, et al. Targeting senescence-like fibroblasts radiosensitizes non–small cell lung cancer and reduces radiation-induced pulmonary fibrosis. JCI Insight. 2021;6(23). doi:10.1172/jci.insight.146334.
28. Kim TK, Vandsemb EN, Herbst RS, Chen L. Adaptive immune resistance at the tumour site: mechanisms and therapeutic opportunities. Nat Rev Drug Discov. 2022;21(7):529–540. doi:10.1038/s41573-022-00493-5.
29. Restifo NP, Smyth MJ, Snyder A. Acquired resistance to immunotherapy and future challenges. Nat Rev Cancer. 2016;16(2):121–126. doi:10.1038/nrc.2016.2.